CrossMark

ORIGINAL PAPER

Oxidation of 5′-dGMP, 5′-dGDP, and 5′-dGTP by a platinum(IV) complex

Ioannis Kipouros[1] · Sebastian Matias Fica-Contreras[1] · Gregory Joon Kee Bowe[1] ·
Sunhee Choi[1]

Abstract We previously reported that a Pt(IV) complex, $[Pt^{IV}(dach)Cl_4]$ [*trans-d,l*-1,2-diaminocyclohexanetetrachloroplatinum(IV)] binds to the N_7 of 5′-dGMP (deoxyguanosine-5′-monophosphate) at a relatively fast rate and oxidizes it to 8-oxo-5′-dGMP. Here, we further studied the kinetics of the oxidation of 5′-dGMP by the Pt^{IV} complex. The electron transfer rate constants between 5′-dGMP and Pt^{IV} in $[H_8\text{-}5'\text{-dGMP–}Pt^{IV}]$ and $[D_8\text{-}5'\text{-dGMP–}Pt^{IV}]$ were similar, giving a small value of the kinetic isotope effect (KIE: 1.2 ± 0.2). This small KIE indicates that the deprotonation of H_8 in $[H_8\text{-}5'\text{-dGMP–}Pt^{IV}]$ is not involved in the rate-determining step in the electron transfer between guanine (G) and Pt^{IV}. We also studied the reaction of 5′-dGDP (deoxyguanosine-5′-diphosphate) and 5′-dGTP (deoxyguanosine-5′-triphosphate) with the Pt^{IV} complex. Our results showed that $[Pt^{IV}(dach)Cl_4]$ oxidized 5′-dGDP and 5′-dGTP to 8-oxo-5′-dGDP and 8-oxo-5′-dGTP, respectively, by the same mechanism and kinetics as for 5′-dGMP. The Pt^{IV} complex binds to N_7 followed by a two-electron inner sphere electron transfer from G to Pt^{IV}. The reaction was catalyzed by Pt^{II} and occurred faster at higher pH. The electron transfer was initiated by either an intramolecular nucleophilic attack by any of the phosphate groups or an intermolecular nucleophilic attack by free OH^- in the solution. The rates of reactions for the three nucleotides followed the order: 5′-dGMP > 5′-dGDP > 5′-dGTP, indicating that the bulkier the phosphate groups are, the slower the reaction is, due to the larger steric hindrance and rotational barrier of the phosphate groups.

Introduction

Oxidation of DNA plays a major role in carcinogenesis [1, 2], aging [3, 4], and neurodegenerative diseases such as Parkinson's and Alzheimer's disease [5, 6]. Among the four nucleobases, guanine (G) has the lowest reduction potential ($E_0 = 1.3$, 1.4, 1.6 and 1.7 V vs. NHE for dGuo, dAdo, dCyt and dThy, respectively) and, therefore, is most easily oxidized [7]. Many transition metal complexes including those of Cr, Mn, Fe, Co, Ni, Cu, Ir, Os, Re, and Rh mediate oxidation of guanine via many different mechanisms and all require oxidizing radiation, photosensitizers, or oxidants [8, 9].

The Ru^{III} and Pt^{IV} complexes can also oxidize purine derivatives, but unlike the oxidation by other transition metal complexes cited above, this process does not involve oxidizing radiation, photosensitizers, or oxidants. Both Ru^{III} and Pt^{IV} complexes are substitution inert but bind slowly to the N_7 of G (N_7) followed by a two-electron inner sphere redox reaction. Clarke's group reported that the H_8 of G (H_8) bound to Ru^{III} (H_8G–Ru^{III}) can be deprotonated by OH^- in basic solution (intermolecular nucleophile), and a two-electron oxidation product of 8-oxo-G is produced in the presence of O_2 molecules [10–12]. Later, our group reported that the H_8 bound to Pt^{IV} {H_8G–Pt^{IV}: $Pt^{IV} = [Pt^{IV}(dach)Cl_4]$} can be deprotonated by 5′-OH or 5′-phosphate (intramolecular nucleophile) forming a two-electron oxidation product of either cyclic-5′-*O*-C8-G or 8-oxo-G without involving O_2 molecules [13, 14]. We also discovered that the redox reaction between Pt^{IV} and G can occur in basic solution or phosphate buffer, where OH^- or

✉ Sunhee Choi
  choi@middlebury.edu

[1] Department of Chemistry and Biochemistry, Middlebury
     College, Middlebury, VT 05753, USA
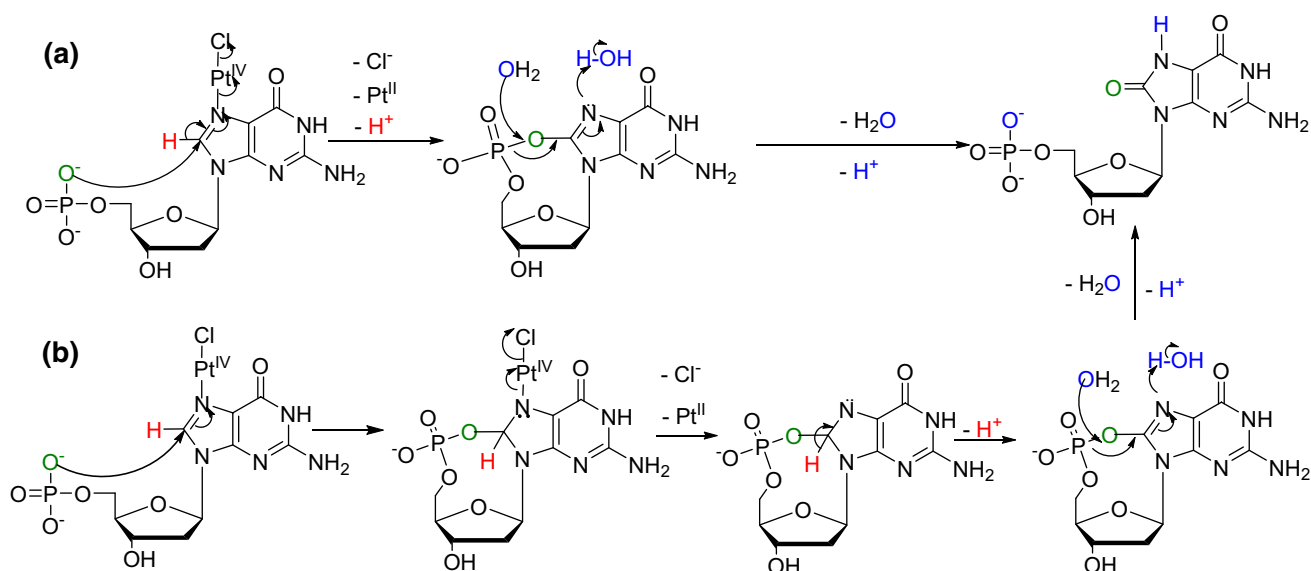
Scheme 1 Proposed mechanism on basis of Choi et al. for the oxidation of 5′-dGMP by [Pt^{IV}(dach)Cl$_4$] [14]. Deprotonation of H$_8$ in **a** is involved in the rate-determining step, but not in **b** [19]

phosphate in solution (intermolecular nucleophile) attacks C$_8$ of G (C$_8$) to produce 8-oxo-G and Pt^{II} [15]. Through this mechanism, every G in the oligonucleotides can be oxidized to 8-oxo-G in phosphate buffer.

We further discovered that Ru^{III} complexes like the Pt^{IV} complex, can go through the two-electron redox mechanism without involving O$_2$ [16, 17]. The [Ru^{III}(NH$_3$)$_5$L] (L = dGuo, dIno, Xao) complex disproportionates in basic solution to the corresponding Ru^{II} and Ru^{IV} complexes, followed by a two-electron redox reaction between Ru^{IV} and L that does not involve O$_2$. When L was dGuo, the two-electron oxidation product was cyclic-5′-O-C8-dGuo [16], but when L was dIno or Xao, the oxidation product was 8-oxo-L [17].

What is the main driving force for the redox reaction between G and Pt^{IV} (and Ru^{III}/Ru^{IV})?

Coordination of a metal ion at N$_7$ inductively withdraws electron density from G, placing a partial positive charge at C$_8$ and promotes the exchange of H$_8$ [18]. Clarke's group showed that the autoxidation rate of [Ru^{III}(NH$_3$)$_5$L] (L = Ino, 1-MeIno, 1-MeGuo, Guo, and dGuo) at high pH to the corresponding 8-oxo complex depends on the polarity of H$_8$ [12]. The change in polarity of C$_8$ is reflected in the chemical shift of H$_8$ of [Ru^{III}(NH$_3$)$_5$L] in the ^{1}H NMR spectra at −31.24, −30.37, and −20.22 ppm for dGuo$^-$, Guo$^-$, and Ino$^-$, respectively. The rate follows the order dGuo < Guo < Ino indicating that the more polar the H$_8$ is, the faster the redox reaction becomes. The oxidation of the 1-MeIno (or 1-MeGuo) complex proceeds approximately 3 times faster than that of the dGuo (or Guo) complex. The H$_8$ of 1-MeGuo is highly susceptible to polarization because there is no H at

N$_1$ to deprotonate at high pH to induce large negative charge on C$_8$. Therefore, the main driving force for the redox reaction should be the polarization of H$_8$ by electron-deficient Pt^{IV} and Ru^{IV}.

One of our major questions in this investigation was at what point the deprotonation of H$_8$ occurs. Does it occur right after the nucleophile attacks C$_8$ (Scheme 1a) or after the two-electron transfer between G and Pt^{IV} is complete (Scheme 1b)? Recent density function theory (DFT) calculations on the oxidation of 5′-dGMP suggested that H$_8$ is deprotonated after the redox reaction (Scheme 1b) [19]. To shed light on which mechanism is more plausible, we determined the kinetic isotope effect (KIE = k_H/k_D) of the electron transfer rate. In Scheme 1a, the rate-determining step is deprotonation of H$_8$, which should give a primary KIE of 7 [20]. On the other hand, in Scheme 1b, the H$_8$ is deprotonated after a two-electron transfer from G to Pt^{IV}, which should give a secondary KIE of a value much smaller than 7. Our results showed that the KIE of *fac*-[Pt^{IV}(dach)Cl$_3$(5′-dGMP)] was 1.2 ± 0.2, indicating that the deprotonation of H$_8$-5′-dGMP–Pt^{IV} is not involved in the rate-determining step. Therefore, the plausible mechanism is not the paths in Scheme 1a but rather in Scheme 1b, which is in agreement with the DFT calculations [19].

Another objective of this study was to investigate the mechanism and kinetics of the oxidation of other nucleotides such as 5′-deoxyguanosine diphosphate (5′-dGDP) and 5′-deoxyguanosine triphosphate (5′-dGTP), and compare them with the conclusions made for the reaction with 5′-dGMP [13–15, 21]. This new objective is biologically important as 5′-dGDP and 5′-dGTP comprise a major

fraction of the intracellular nucleotide pool, and their modification by transitional metal complexes can lead to mutations through their incorporation in the DNA chain during replication. These indirect modifications of the DNA molecule could cause mutagenesis in the same fashion as the direct modification of the normal guanine bases of DNA [22]. Our results showed that $[Pt^{IV}(dach)Cl_4]$ oxidized 5′-dGDP and 5′-dGTP to 8-oxo-5′-dGDP and 8-oxo-5′-dGTP, respectively, by the same mechanism and kinetics as in the case of 5′-dGMP [13–15, 21]. The Pt^{IV} complex binds to N_7 followed by a two-electron inner sphere electron transfer from G to Pt^{IV}. The reaction was catalyzed by Pt^{II} and occurred faster at higher pH. The electron transfer was initiated by either an intramolecular nucleophilic attack by any of the phosphate groups or an intermolecular nucleophilic attack by free $OH^−$ in the solution. The rates of reactions for the three nucleotides followed the order: 5′-dGMP > 5′-dGDP > 5′-dGTP, indicating that the bulkier the phosphate groups are, the slower the reaction is, due to the larger steric hindrance and rotational barrier of the phosphate groups.

Materials and methods

Chemicals

$[Pt^{IV}(dach)Cl_4]$ was obtained from the National Cancer Research Institute, Drug Synthesis and Chemistry Branch, Development Therapeutics Program, Division of Cancer Treatment. The deoxy-nucleotides, 5′-dGMP (>99 %) and 5′-dGDP (>90 %) were obtained from Sigma-Aldrich, and 5′-dGTP (>98 %) was obtained from GE Healthcare Life Science, and were all used as sodium salts. NaCl, NaOH, HCl, ammonium acetate, and HPLC-grade acetonitrile were purchased from Fisher Scientific. Radiolabeled $H_2^{18}O$ (97 %) was purchased from Berry & Associates, Synthetic Medicinal Chemistry. All other chemicals were obtained from Sigma-Aldrich. All chemicals were used as purchased without any further purification. All water used was purified by a Hydro Picotech 2 purification system. The pH of reactions and solvents was adjusted with 1.0 M NaOH and 0.5 M HCl, using an Orion Research Expandable Ion Analyzer EA 940 equipped with Corning Semi-Micro Combo electrode. For NMR experiments D_2O (99.9 %) was used as the solvent, and the pH of the solution samples was adjusted with 1.0 M NaOD (99.9 %), both chemicals were obtained from Sigma-Aldrich.

Synthesis of D_8-5′-dGMP

D_8-5′-dGMP was prepared by adapting a previously published procedure [23]. Briefly, 0.0203 g 5′-dGMP was dissolved in 5 mL of D_2O and heated at 80 °C for 24 h. The solution was dried under N_2 gas, and a white solid was collected. The solid was isolated by vacuum filtration and identified by ^1H NMR and ESI-LC/MS. The ^1H NMR peak at 8.3 ppm corresponding to the H_8G of 5′-dGMP had disappeared and the ESI-LC/MS showed an m/z peak of 348.5 (m/z for 5′-dGMP = 347.5), indicating that the reaction was completed and the 5′-dGMP was completely deuterated.

Preparation of reactions

Stock solutions of $[Pt^{IV}(dach)Cl_4]$ (10 mM) were prepared by dissolving appropriate amounts of $[Pt^{IV}(dach)Cl_4]$ in water (in the form of $H_2^{16}O$, $H_2^{18}O$, or D_2O) followed by stirring and gentle heating (maximum 50 °C) for at least 6 h. An appropriate amount of NaCl was also added to a final concentration of 100 mM to decrease the hydrolysis of $[Pt^{IV}(dach)Cl_4]$ through the replacement of its chloride ligands by water. When needed $[Pt^{II}(dach)Cl_2]$ was also dissolved in the solution in low concentrations (~0.02 mM). A fresh solution of $[Pt^{IV}(dach)Cl_4]$ was prepared for each reaction as $[Pt^{IV}(dach)Cl_4]$ hydrolyzes when in solution for extended periods of time. Buffers were not used to avoid complications arising from buffer coordination to platinum. Appropriate amounts of 5′-dGMP, 5′-dGDP or 5′-dGTP were weighted in 1.5-mL Eppendorf tubes, in which the desired volume of the dissolved $[Pt^{IV}(dach)Cl_4]$ solution was transferred. The solution was vortexed for 5 min and the pH was then raised to 7.0 or 8.6 using 1.0 M NaOH (or NaOD). Each solution was then incubated at 37 °C in a Teckam Dri-Block with a DB-1 Heater, while covered in aluminum foil to avoid any form of photodegradation. All the samples for NMR analysis were prepared in D_2O (>98 %). Most reaction solutions were filtered through a syringe-end filter disk (Gelman Acrodisk 0.45 μm pore size) before ESI-LC/MS and NMR analysis.

^1H and ^{31}P NMR spectroscopy

NMR spectra were recorded on a Bruker 400 Ultrashield spectrometer in D_2O at room temperature. The ^1H NMR spectra of all reactions were taken at 400.1319 MHz over 50–256 scans. No water-suppression method was used, since the peaks of interest had chemical shifts that were not close to that for water. For the ^{31}P NMR spectra, 2000 scans were taken at 16233.77 Hz. All free inductions decays (FID) were Fourier transformed and analyzed using Bruker TOPSPIN 1.3 software. Spectra were edited using the XWIN-PLOT software.

Electron spray ionization–liquid chromatography/mass spectrometry (ESI-LC/MS)

Liquid chromatography coupled to a mass spectrometer was used to identify the intermediates and final oxidation

products of the reactions. A 1100 Series LC, coupled to an LC-MSD Trap XCT Plus system from Agilent Technologies, was used to perform sample analysis. The liquid chromatography component was equipped with a photo diode array detector and an Eclipse X-D8-C8 column. Isocratic elution was performed with 0.5 % aqueous formic acid solution at a flow rate of 0.5 mL/min. The mass spectrometer was set to scan in the range of 50–2200 m/z, detecting positive ions with electrospray ionization mass spectrometry (ESI–MS). The nitrogen nebulizer pressure was set to 50 psi, the dry gas (helium) flow to 9 L/min, and the dry temperature to 365 °C. The ion trap was set to collect targeted molecules and acquire their fragmentation mass spectra.

UV/Vis spectroscopy

UV/Vis spectroscopy was used to monitor the reaction rates of $[Pt^{IV}(dach)Cl_4]$ with 5′-dGMP, 5′-dGDP and 5′-dGTP. UV/Vis spectra were obtained in 10-mm-path length micro quartz cells on a Varian Cary 4000 Spectrophotometer with Cary Win UV kinetic assay software. All kinetic experiments were replicated at least in triplicate. The baseline absorbance was measured using water prior to experimental measurements. Analysis of the obtained kinetic data was performed using the Kaleidagraph software.

Results and discussion

Kinetic isotope effect of the reaction of 5′-dGMP with $[Pt^{IV}(dach)Cl_4]$

Figure 1 compares the kinetic curves of the reaction of H_8-5′-dGMP and D_8-5′dGMP with $[Pt^{IV}(dach)Cl_4]$ at pH 7.0 and 40 °C. Both reactions show the same kinetics trends.

$$Pt^{IV}\text{–}Cl + G + Pt^{II} \xrightarrow{k_s} Pt^{IV}\text{–}G + Pt^{II} \qquad (1)$$

$$Pt^{IV}\text{–}G \xrightarrow{k_e} Pt^{II} + G\,(\text{-}2e) \qquad (2)$$

Scheme 2 Kinetic model for the oxidation of G by $[Pt^{IV}(dach)Cl_4]$[13]

As indicated by the decrease in A_{360}, the disappearance of the reactant, $[Pt^{IV}(dach)Cl_4]$, is slow in the beginning, but increases in rate as the reaction progresses because the reaction is auto-catalyzed by the product, $[Pt^{II}(dach)Cl_2]$. The A_{390} curve arises from the intermediate, fac-$[Pt^{IV}(dach)(5′\text{-}dGMP)Cl_3]^+$. The kinetic curves of A_{360} and A_{390} vs. time were fitted with the DynaFit Software [24] utilizing the kinetic model in Scheme 2 [21]. The substitution rate constant (k_s) and the electron transfer rate constant (k_e) giving the best fit to both A_{360} and A_{390} curves were identical.

The k_s and k_e values giving the best fit to the curves of A_{360} and A_{390} (Fig. 1) were basically the same for H_8-5′-dGMP and D_8-5′-dGMP. The k_s of H_8-5′-dGMP and D_8-5′-dGMP at pH 7.0 and 40 °C were 5.02 ± 0.88 and 4.76 ± 0.07 $M^{-2}s^{-1}$, respectively. The k_e of H_8-5′-dGMP and D_8-5′-dGMP at pH 7.0 and 40 °C were 3.13 (±0.08) × 10^{-4} s^{-1} and 3.06 (±0.03) × 10^{-4} s^{-1}, respectively. These rate constants are comparable with the previously found k_s and k_e values of 5′-dGMP at pH 8.3 and 40 °C, which were 8.1 ± 0.2 $M^{-2}s^{-1}$ and 3.6 (±0.5) × 10^{-4} s^{-1}, respectively [21]. The kinetic isotope effect (KIE) of k_e which is the ratio of the k_e of H_8-5′-dGMP to the k_e of D_8-5′-dGMP was calculated to be 1.2 ± 0.2. This small KIE value suggests that the deprotonation of H_8 bound to Pt^{IV}, [H_8-5′-dGMP–Pt^{IV}], is not involved in the rate-determining step in the electron transfer between G and Pt^{IV}. This result is consistent with the DFT calculation which predicted that H_8 deprotonates after two electrons from 5′-dGMP are transferred to Pt^{IV}, the rate-determining step in the electron transfer (Scheme 1b) [19].

Fig. 1 Kinetic curves at **a** 360 and **b** 390 nm of the reactions of $[Pt^{IV}(dach)Cl_4]$ with H_8-5′-dGMP and D_8-5′-dGMP in 100 mM NaCl at 40 °C with a starting pH 7.0 ($t = 0$). Fits to both A_{360} and A_{390} curves give identical k_s and k_e values

It is interesting to note that the KIE of k_e of *fac*-[Pt^{IV}(dach)(9-EtG)Cl$_3$]$^+$ (9-EtG = 9-ethylguanine) at high pH (pH 12) is reported to be 7.2 ± 0.2 [16]. At high pH, the electron transfer is initiated by OH$^-$ in the solvent (inter molecular nucleophile), while at pH 7, the electron transfer is initiated by 5′-phosphate (intramolecular nucleophile). These results indicate that OH$^-$ is a more powerful nucleophile than phosphate. However, the KIE of autoxidation of [Ru^{III}(NH$_3$)$_5$(Ino)] assisted by O$_2$ and OH$^-$ is reported to be a secondary KIE of 1.6 [11]. It seems that different systems have different KIEs, indicating that deprotonation occurs at different stages, depending on the nucleophiles involved.

Reaction of 5′-dGDP with [Pt^{IV}(dach)Cl$_4$]

The time course of the reaction of [Pt^{IV}Cl$_4$(dach)]/5′-dGDP (10/20 mM) was monitored by ^{1}H-NMR spectroscopy, and the results were in parallel with those for 5′-dGMP [14]. Figure 2 shows the ^{1}H NMR spectra in the area where the chemical shifts of H$_8$ and H$_{1'}$ appear. When G is free, H$_8$ resonates around 8.2 ppm (not shown). When G is bound to the electron-deficient Pt^{IV} and Pt^{II} at the N$_7$ position, the chemical shifts of H$_8$ change to 9.03 and 8.32 ppm, respectively. The 9.03 ppm peak appears after 12 h and disappears after around 48 h, indicating that Pt^{IV}-bound G is an intermediate. The 8.32 ppm peak appears after 24 h and grows in intensity, indicating that the Pt^{II}-bound G is a product.

The H$_{1'}$ of free G resonates at 6.17 ppm. The two overlapping peaks around 6.33 ppm correspond to the second intermediates and were assigned to the H$_{1'}$ of the cyclic (5′-PO-C8)-dGDP intermediate, one involving the

α-phosphate in the ring structure, and the other one the β-phosphate. At 24 h the peak at 6.33 ppm appears as a triplet with no overlapping, suggesting that one cyclic intermediate is more stable than the other and disappears faster. The peaks at 6.10 and 6.15 ppm arise from H$_{1'}$ of the final products of 8-oxo-dGDP and Pt^{II}-bound-5′-dGDP, respectively.

Figure 3 shows an overlay of the time course of ^{31}P-NMR spectra of the reaction of 5′-dGDP (20 mM) with [Pt^{IV}(dach)Cl$_4$] (10 mM) in D$_2$O with 100 mM NaCl and a starting pH of 8.6. At the beginning of the reaction ($t = 0$ h) there are two doublets at −5.95 and −10.20 ppm corresponding to the resonance of ^{31}P nuclei of the β- and α-phosphate groups of free 5′-dGDP, respectively [25]. The ^{31}P peak of the β-phosphate of free 5′-dGDP at −5.95 ppm shifts upfield over the course of the reaction to −9.0 ppm after 48 h. This upfield chemical shift is due to the protonation of the phosphate group (pK$_a$ = 6.8), as the pH of the reaction mixture decreases over time due to the production of two protons in the two-electron redox reaction [13, 14]. It is known that both inorganic and nucleotide phosphates shift upfield when phosphate is protonated [26, 27]. After 12 h of reaction two new doublets are formed at −11.3 and −19.0 ppm and gradually disappear. These are assigned to the (5′-P$_\beta$O-C8)-dGDP and (5′-P$_\alpha$O-C8)-dGDP cyclic intermediates, respectively. The upfield chemical shifts of 5 and 9 ppm of (5′-P$_\beta$O-C8)-dGDP and (5′-P$_\alpha$O-C8)-dGDP, respectively, compared to the free 5′-dGDP, are relatively close to that of 10 ppm upfield reported for the cyclic intermediate in 5′-dGMP. The ^{31}P peaks of free 5′-dGMP and (5′-PO-C8)-dGMP appear around 5.0 and −5.5 ppm, respectively [14].
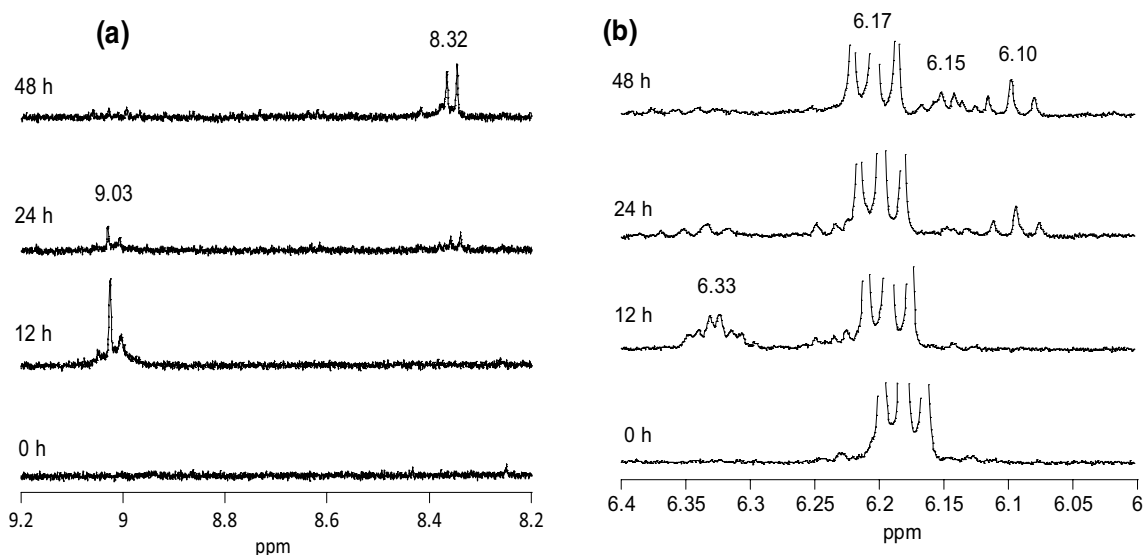

Fig. 2 Time-dependent ^{1}H NMR spectra of the reaction of 10 mM [Pt^{IV}Cl$_4$(dach)] with 20 mM 5′-dGDP in 100 mM NaCl at 37 °C with a starting pH 8.6 ($t = 0$)
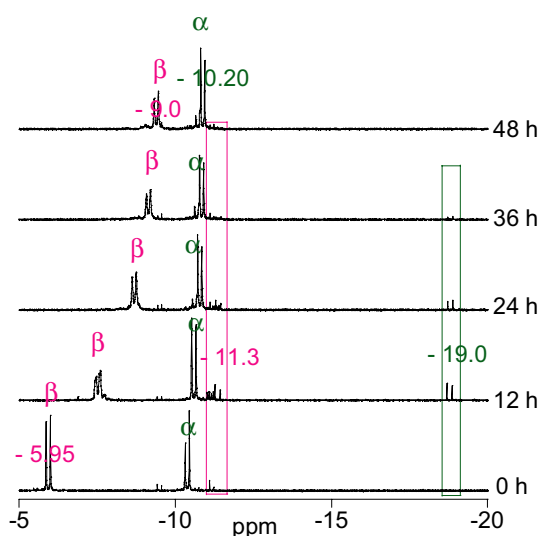
Fig. 3 Time-dependent ^{31}P NMR spectra of the reaction of 10 mM [Pt^{IV}Cl$_4$(dach)] with 20 mM 5′-dGDP in 100 mM NaCl at 37 °C with a starting pH 8.6 ($t = 0$)

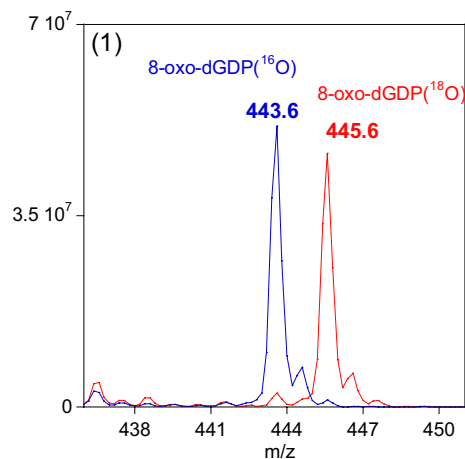**Fig. 4** Mass spectrum of *fac*-[Pt^{IV}(dach)(5′-dGDP)Cl$_3$] along with its theoretical isotope patterns

Fig. 5 Mass spectra of 8-oxo-5′-dGDP produced from the reaction mixture of 5′-dGDP (20 mM) with [Pt^{IV}(dach)Cl$_4$] (10 mM) in (a) H$_2^{16}$O and (b) H$_2^{18}$O in 100 mM NaCl after 48 h at 37 °C with a starting pH 8.6 ($t = 0$)

Two more doublets, with low intensities, appear after 12 h of reaction with chemical shifts 0.5 ppm upfield from the peaks of α and β-phosphate of free 5′-dGDP. These peaks probably correspond to the ^{31}P nuclei of the neighboring phosphate groups in the two cyclic intermediates, which do not participate in the phosphodiester bond. This assignment is supported by the fact that these low-intensity peaks show up in the same timeframe with the other two intermediate peaks, and have significantly smaller changes in chemical shifts, as expected for nuclei that do not participate directly in chemical changes in the molecule. It is also possible that these peaks correspond to the Pt^{IV}–dGDP intermediate.

To further verify the identity and presence of the Pt^{IV}–dGDP intermediate, the above reaction mixture was analyzed by ESI-LC/MS. Figure 4 shows the mass spectrum of Pt^{IV}–dGDP obtained after 16 h of reaction. The major peak 841.5 (m/z) is close to the expected mass of Pt^{IV}–dGDP (840.0 amu). The multiple surrounding peaks appear due to the several platinum isotopes.

To confirm the ^{31}P NMR results indicating that both phosphate groups (α and β) participate in the intramolecular nucleophilic attack to produce the cyclic phosphodiester intermediate, the reactions of [Pt^{IV}(dach)Cl$_4$] with 5′-dGDP were carried out in both normal H$_2^{16}$O and H$_2^{18}$O and their products were analyzed by ESI-LC/MS. In particular, the fragmentation mass spectra of 8-oxo-dGDP from both reactions after 48 h were obtained and analyzed. Figure 5 shows the overlay of the mass spectra of 8-oxo-5′-dGDP obtained from the reaction in H$_2^{16}$O (8-oxo-5′-dGDP(^{16}O)) and 8-oxo-5′-dGDP obtained from the reaction in H$_2^{18}$O

[8-oxo-dGDP(^{18}O)]. The mass of 8-oxo-5′-dGDP(^{18}O) (445.6 m/z) is 2 amu higher than the mass of 8-oxo-5′-dGDP(^{16}O) indicating that the former compound contains an ^{18}O atom in its structure. The absence of a peak at 443.6 (m/z) in the reaction in H$_2^{18}$O suggests that there was not any significant contamination by H$_2^{16}$O. Furthermore, the mass of 5′-dGDP from a control experiment of incubating 5′-dGDP in H$_2^{18}$O without [Pt^{IV}(dach)Cl$_4$] for 48 h did not increase 2 amu. This result confirmed that the 2 amu increase of 8-oxo-5′-dGDP(^{18}O) was not due to the oxygen exchange in the phosphates of 5′-dGDP, but due
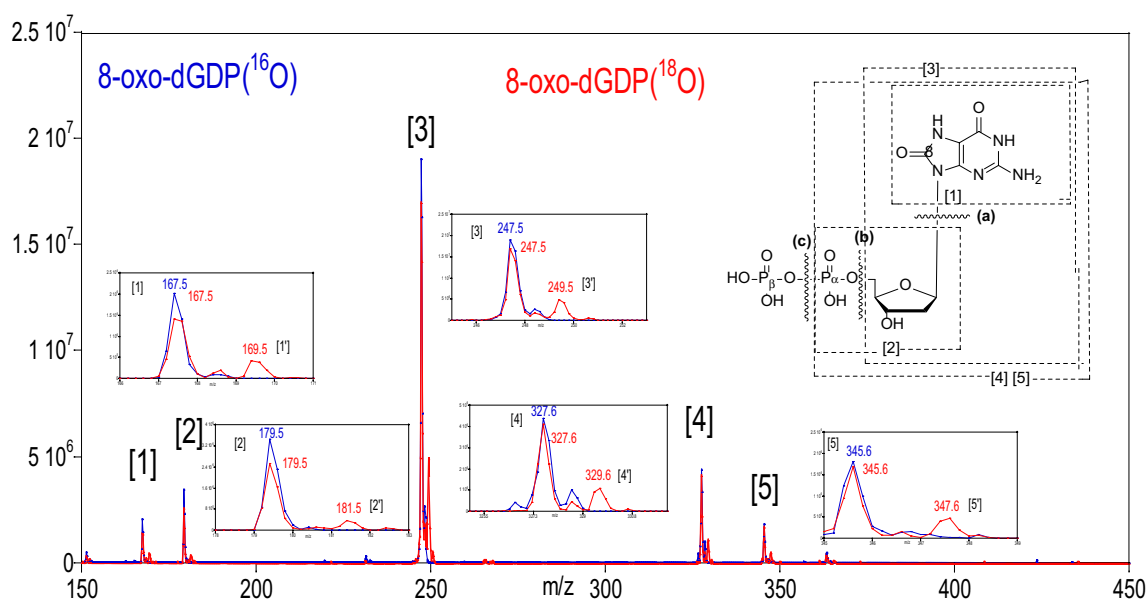
Fig. 6 Fragmentation mass spectra of 8-oxo-5′-dGDP obtained from the reaction mixture of 5′-dGDP (20 mM) with [Pt^{IV}(dach)Cl$_4$] (10 mM) in **a** H$_2$O^{16} and **b** H$_2$O^{18} in 100 mM NaCl after 48 h at 37 °C with a starting pH 8.6 (*t* = 0). *Inset* structure of 5′-dGDP along with the bond breaking positions

to the involvement of H$_2^{18}$O in the reaction of [Pt^{IV}(dach) Cl$_4$] and 5′-dGDP. Similarly, the absence of any peaks corresponding to a mass higher than 8-oxo-5′-dGDP(^{16}O) by 4 or 6 amu further indicates that oxygen in water did not exchange in the phosphates of 5′-dGDP.

Figure 6 displays the overlay of fragmentation mass spectra of 8-oxo-5′-dGDP(^{16}O) and 8-oxo-5′-dGDP(^{18}O) from *m/z* 150 to 450. The fragmentation mass spectrum of 8-oxo-5′-dGDP(O^{16}) shows five major peaks arising from fragments [1], [2], [3], [4], and [5]. All of these peaks appear in 8-oxo-5′-dGDP(^{18}O) as well, accompanied by the corresponding weaker peaks at 2 amu higher arising from fragments [1′], [2′], [3′], [4′], and [5′]. The structure of 8-oxo-5′-dGDP, the possible bond breakages, and the five fragments are shown in the inset in Fig. 6. When the bonds break at (a) and (c) positions, the fragments [1] and [2] are produced. The fragment [1] with *m/z* = 167.5 due to guanine can be generated from both 8-oxo-5′-dGDP(^{16}O) and 8-oxo-5′-dGDP(^{18}OP$_\beta$) or 8-oxo-5′-dGDP(^{18}OP$_\alpha$), but [1′] with *m/z* = 169.5 can be generated only from 8-oxo-5′-dGDP(^{18}OC$_8$). The fragment [2] with *m/z* = 179.5 due to ribose-phosphate can be generated from both 8-oxo-5′-dGDP(^{16}O) and 8-oxo-5′-dGDP(^{18}OP$_\beta$) or, 8-oxo-5′-dGDP(^{18}OC$_8$), but [2′] with *m/z* = 181.5 from 8-oxo-5′-dGDP(^{18}OP$_\alpha$). When the bond breaks at (b), the fragment [3] with *m/z* = 247.5 due to guanosine is generated from both 8-oxo-5′-dGDP(^{16}O) and 8-oxo-5′-dGDP(^{18}OP$_\beta$) or 8-oxo-5′-dGDP(^{18}OP$_\alpha$), but [3′] with *m/z* = 249.5 from 8-oxo-5′-dGDP(^{18}OC$_8$). When the bond breaks at (c), the fragments [4] and [5] with *m/z* = 327.6 and 345.6, respectively, from

8-oxo-5′-dGDP(^{16}O) and 8-oxo-5′-dGDP(^{18}OP$_\beta$) are generated, while fragments [4′] and [5′] with *m/z* = 329.6 and 347.6, are generated, respectively, from 8-oxo-5′-dGDP(^{18}OP$_\alpha$) or 8-oxo-5′-dGDP(^{18}OC$_8$). These results clearly indicate that ^{18}O atom in 8-oxo-5′-dGDP(^{18}O) can be located at P$_\beta$, P$_\alpha$, or C$_8$, indicating that both an intermolecular and an intramolecular nucleophilic attack to the Pt(IV)– G intermediate is possible. The possible structures of all the fragments along with their *m/z* are summarized in Table 1.

Together the ^{1}H and ^{31}P NMR, and ESI–MS/MS studies led us to propose the mechanism in Scheme 3. The [Pt^{IV}(dach)Cl$_4$] complex binds to the N$_7$ and a two-electron transfer from G to Pt^{IV} occurs. The two-electron transfer step is initiated by an intramolecular nucleophilic attack by either the α or β phosphate groups followed by cyclization and hydrolysis, or by an intermolecular nucleophilic attack by OH$^-$.

Reaction of 5′-dGTP with [Pt^{IV}(dach)Cl$_4$]

The time course of the reaction of [Pt^{IV}Cl$_4$(dach)]/5′-dGTP (10/20 mM) was monitored by ^{1}H-NMR spectroscopy, and the results were in parallel with those for 5′-dGMP [14] and 5′-dGDP described above. Figure 7 shows the ^{1}H NMR spectra in the area where the chemical shifts of H$_8$ and H$_{1'}$ of guanosine (G) occurs. The H$_8$ peak due to Pt^{IV}-bound dGTP appears at 9.00 ppm, and the Pt^{II}-bound dGTP peak at 8.35 ppm. The H$_{1'}$ peaks due to the cyclic (5′-PO-C8)-dGTP intermediate, 8-oxo-dGTP, and Pt^{II}-bound dGTP appear at 6.29, 6.07, and 6.13 ppm, respectively.

Table 1 Possible structures of fragments of 8-oxo-5′-dGDP corresponding to the peaks in Fig. 6
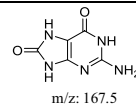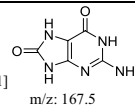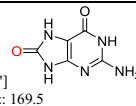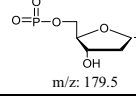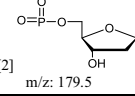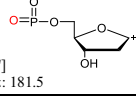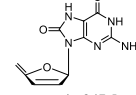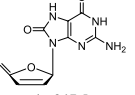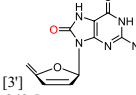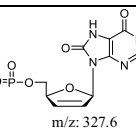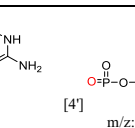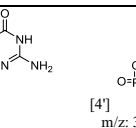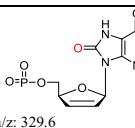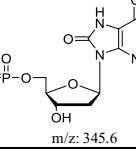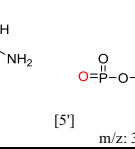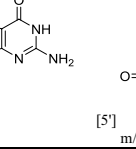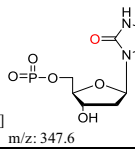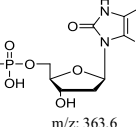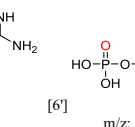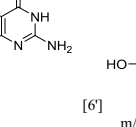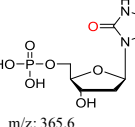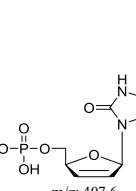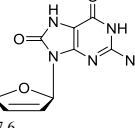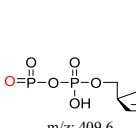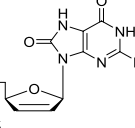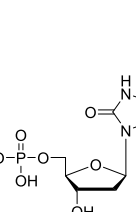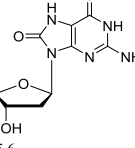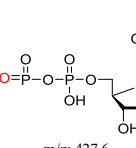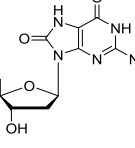
H_2O^{16}	H_2O^{18}		
[1] m/z: 167.5	[1] m/z: 167.5	[1'] m/z: 169.5	
[2] m/z: 179.5	[2] m/z: 179.5	[2'] m/z: 181.5	
[3] m/z: 247.5	[3] m/z: 247.5	[3'] m/z: 249.5	
[4] m/z: 327.6	[4] m/z: 327.6	[4'] m/z: 329.6	[4'] m/z: 329.6
[5] m/z: 345.6	[5] m/z: 345.6	[5'] m/z: 347.6	[5'] m/z: 347.6
[6] m/z: 363.6	[6] m/z: 363.6	[6'] m/z: 365.6	[6'] m/z: 365.6
[7] m/z: 407.6	[7] m/z: 407.6 / [7'] m/z: 409.6	[7'] m/z: 409.6 / [7'] m/z: 409.6	
[8] m/z: 425.6	[8] m/z: 425.6 / [8'] m/z: 427.6	[8'] m/z: 427.6 / [8'] m/z: 427.6	

Figure 8 shows an overlay of the ^{31}P-NMR spectra of the reaction of 5′-dGTP (20 mM) with [Pt^{IV}(dach)Cl$_4$] (10 mM) in D$_2$O with 100 mM NaCl and a starting pH of 8.6, without the presence of buffer, at different times. At the beginning of the reaction, the doublets at −10.6 and −5.5 ppm correspond to α and γ phosphate groups of free 5′-dGTP, respectively, and the triplet at 21.1 ppm to the ^{31}P nuclei of the β phosphate. This assignment is in agreement with previously published studies [25]. The chemical shift corresponding to the γ-phosphate of free 5′-dGTP
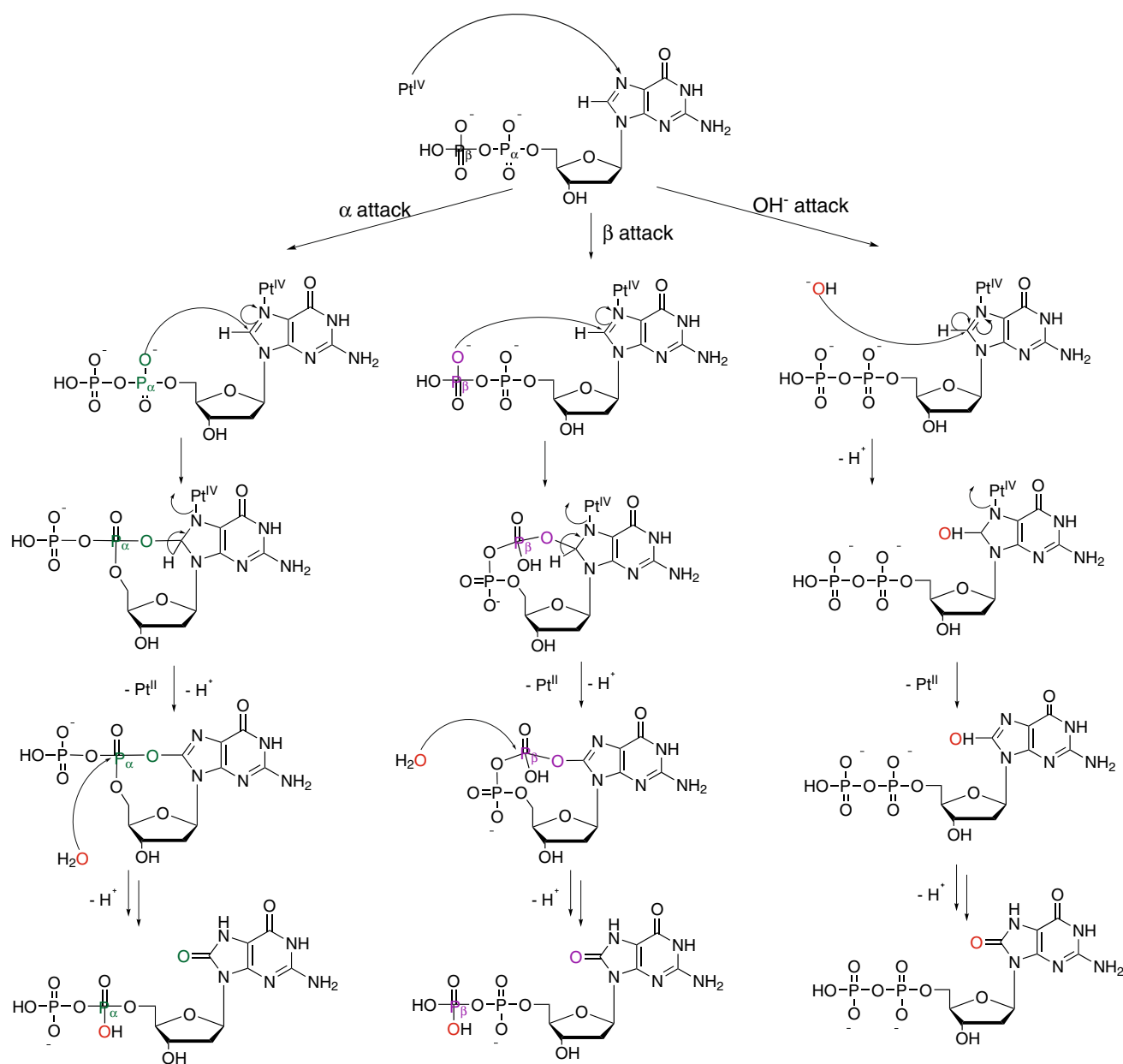
Scheme 3 Proposed mechanism for the oxidation of 5′-dGDP by [Pt^{IV}(dach)Cl$_4$] (represented as Pt^{IV}). [Pt^{II}(dach)Cl$_2$] is represented as Pt^{II}. The [Pt^{II}(dach)Cl$_2$] complex reacts further with excess 5′-dGDP and produces [Pt^{II}(dach)(5′-dGDP)$_2$]

shifts upfield over the course of the reaction to −8.1 ppm after 36 h. This upfield chemical shift is due to the protonation of the phosphate group (pKa ~ 6.7), as the pH of the reaction mixture decreases over time [26, 27]. After 12 h of reaction, two new doublets are formed at −19.7 and −11.35 ppm, and a triplet at −23.7 ppm, all of which gradually disappear over time. They were assigned to the ^{31}P nuclei of the participating in the phosphodiester bond in the cyclic intermediates (5′-P$_\gamma$O-C8)-dGTP, (5′-P$_\alpha$O-C8)-dGTP, and (5′-P$_\beta$O-C8)-dGTP, respectively. After 12 h of reaction, low-intensity peaks appear with chemical shifts of

0.5 ppm upfield from the corresponding peaks of α, β, and γ-phosphate of free 5′-dGTP. These peaks probably correspond to the ^{31}P nuclei of the neighboring phosphate groups in the two cyclic intermediates, which do not participate in the phosphodiester bond, or due to the peaks arising from the binding of [Pt^{IV}(dach)Cl$_4$] to the N$_7$ of 5′-dGTP.

To further verify the identity and presence of the Pt^{IV}–dGTP intermediate, the above reaction mixture was analyzed by ESI-LC/MS. Figure 9 shows the mass spectrum of Pt^{IV}–dGTP obtained after 16 h of reaction. The major peak 921.5 (*m/z*) is close to the expected mass of Pt^{IV}–dGTP
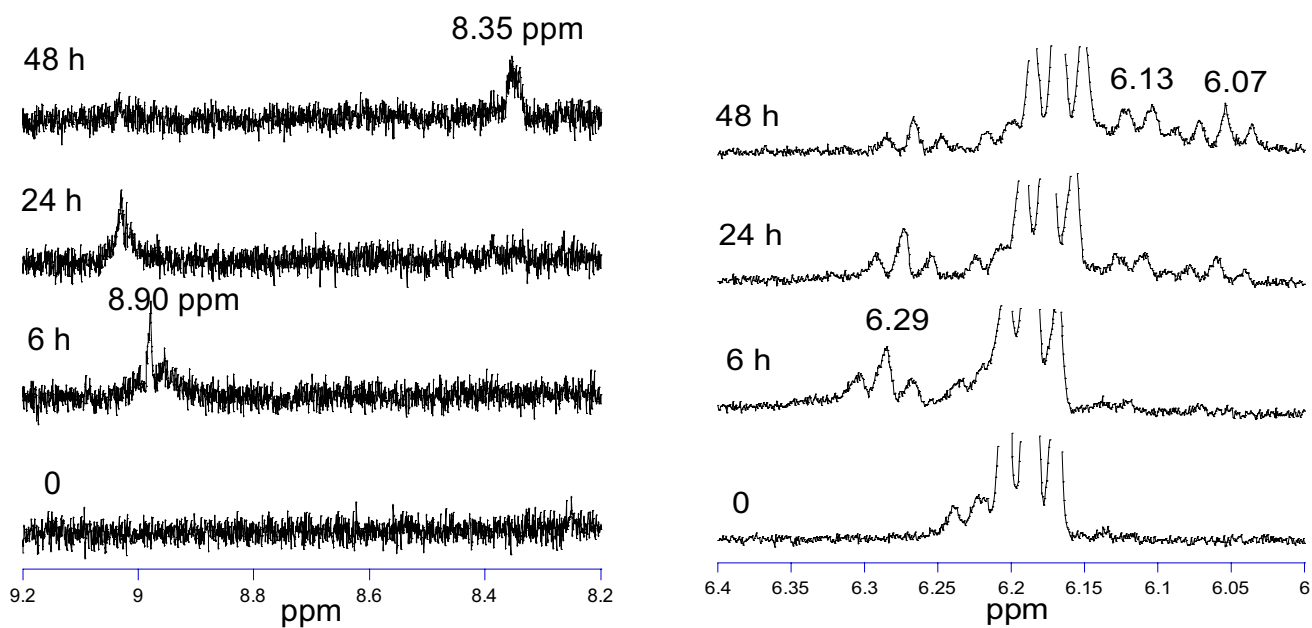
Fig. 7 Time-dependent ^{1}H NMR spectra of the reaction of 10 mM [Pt^{IV}Cl$_4$(dach)] with 20 mM 5′-dGTP in 100 mM NaCl at 37 °C with a starting pH 8.6 ($t = 0$)

Fig. 8 Time-dependent ^{31}P NMR spectra of the reaction of 10 mM [Pt^{IV}Cl$_4$(dach)] with 20 mM 5′-dGTP in 100 mM NaCl at 37 °C with a starting pH 8.6 ($t = 0$). **a** −5 to −25 ppm ran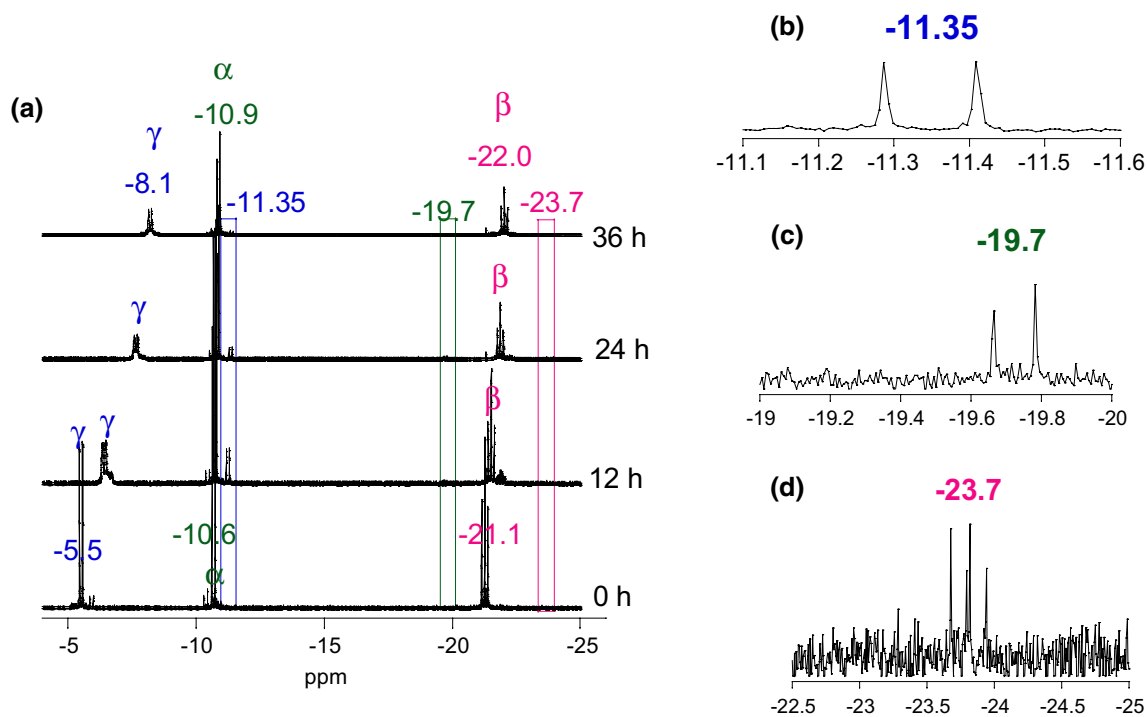ge; **b** −11.1 to −11.6 ppm range after 24 h; **c** −19 to −20 ppm range after 24 h; **d** −22 to −23.5 ppm range after 24 h
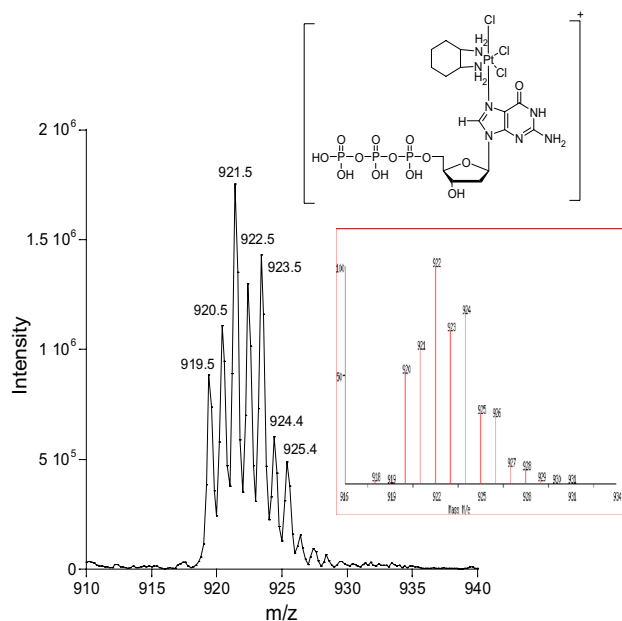
Fig. 9 Mass spectrum of *fac*-[Pt^{IV}(dach)(5′-dGTP)Cl$_3$] along with its theoretical isotope pattern

Fig. 10 Mass spectra of 8-oxo-5′-dGTP produced from the reaction mixture of 5′-dGTP (20 mM) with [Pt^{IV}(dach)Cl$_4$] (10 mM) in **a** H$_2^{16}$O and **b** H$_2^{18}$O in 100 mM NaCl after 48 h at 37 °C with a starting pH 8.6 ($t = 0$)

(920.0 amu). The multiple surrounding peaks appear due to the several platinum isotopes.

To confirm the ^{31}P NMR results indicating that all three phosphate groups (α, β, and γ) participate in the intramolecular nucleophilic attack to produce the cyclic phosphodiester intermediate, the reactions of [Pt^{IV}(dach)Cl$_4$] with 5′-dGTP were carried out in both normal H$_2^{16}$O and H$_2^{18}$O and the results were analyzed by ESI-LC/MS. In particular, the fragmentation mass spectra of 8-oxo-dGTP from both reactions after 48 h were obtained and analyzed.

Figure 10 shows the mass spectra of 8-oxo-5′-dGTP obtained from the reaction in H$_2^{16}$O [8-oxo-5′-dGTP(^{16}O)] and 8-oxo-5′-dGTP obtained from the reaction in H$_2^{18}$O [8-oxo-5′-dGTP(^{18}O)]. The mass of 8-oxo-5′-dGTP(^{18}O) (525.5 m/z) is higher than the mass of 8-oxo-5′-dGTP(^{16}O) by 2 amu indicating that the former compound contains an ^{18}O atom in its structure. The absence of a peak at 523.5 (*m/z*) in the reaction in H$_2^{18}$O suggests that there was not any significant contamination by H$_2^{16}$O. Furthermore, the mass of 5′-dGTP from a control experiment of incubating 5′-dGTP in H$_2^{18}$O without [Pt^{IV}(dach)Cl$_4$] for 48 h did not increase 2 amu. This result confirmed that the 2 amu increase of 8-oxo-5′-dGTP(^{18}O) was not due to the oxygen exchange in the phosphates of 5′-dGTP, but due to the involvement of H$_2^{18}$O in the reaction of [Pt^{IV}(dach)Cl$_4$] and 5′-dGTP. Similarly, the absence of any peaks corresponding to a mass higher than 8-oxo-dGTP(^{16}O) by 4 or 6 amu further indicates that oxygen in water did not exchange in the phosphates of 5′-dGTP.
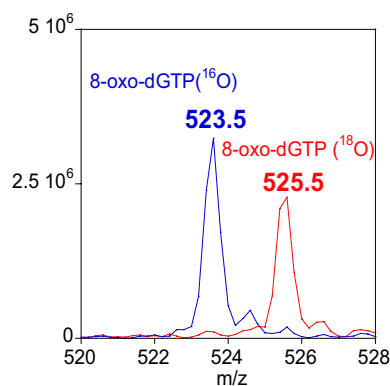
Figure 11 displays the overlay of fragmentation mass spectra of 8-oxo-5′-dGTP(^{16}O) and 8-oxo-5′-dGTP(^{18}O) from *m/z* 150 to 450. The fragmentation mass spectrum of 8-oxo-5′-dGTP(^{16}O) shows eight major peaks arising from fragments [1], [2], [3], [4], [5], [6], [7], and [8]. All these peaks appear in 8-oxo-dGTP(^{18}O) as well, accompanied by the corresponding weaker peaks at 2 amu higher arising from fragments [1′], [2′], [3′], [4′], [5′], [6′], [7′], and [8′]. The structure of 8-oxo-5′-dGTP, possible bond breakages, and eight fragments are shown in the inset in Fig. 11. The fragments [1] to [5] were generated exactly the same way as for the 5′-dGDP. The fragments [7] and [8] indicate that an ^{18}O atom should reside at P$_\gamma$ and the fragment [7′] and [8′] should contain ^{18}O at P$_\beta$, P$_\alpha$, or C$_8$.

Together, the ^{1}H and ^{31}P NMR, and ESI–MS/MS studies led us to propose the mechanism in Scheme 4. The [Pt^{IV}(dach)Cl$_4$] complex binds to the N$_7$, followed by a two-electron transfer from G to Pt^{IV}. The two-electron transfer step is initiated by an intramolecular nucleophilic attack by either the α, β, or γ phosphate group followed by cyclization and hydrolysis, or by an intermolecular nucleophilic attack by OH$^-$.

Kinetics of the reaction of 5′-dGMP, 5′-dGDP and 5′-dGTP with [Pt^{IV}(dach)Cl$_4$]

Figure 12 shows the changes in the electronic absorption at 360 and 390 nm over time, for the reaction of [Pt^{IV}(dach)Cl$_4$] with 5′-dGMP, 5′-dGDP, and 5′-dGTP at 35 °C and at a starting pH of 8.6. The changes in the electronic absorption at 360 nm (A_{360}) indicate the depletion of the unbound [Pt^{IV}(dach)Cl$_4$], while those at 390 nm (A_{390}) the formation and depletion of the Pt^{IV}–G intermediate. The change in A_{360} of 5′-dGMP is significantly larger than that of 5′-dGDP, which in turn is higher than that of 5′-dGTP. This trend suggests that [Pt^{IV}(dach)Cl$_4$] reacts faster with 5′-dGMP,

Fig. 11 Fragmentation mass spectra of 8-oxo-5′-dGTP obtained from the reaction mixture of 5′-dGTP (20 mM) with [Pt^{IV}(dach)Cl$_4$] (10 mM) in **a** H$_2^{16}$O and **b** H$_2^{18}$O in 100 mM NaCl after 48 h at 37 °C with a starting pH 8.6 ($t = 0$)
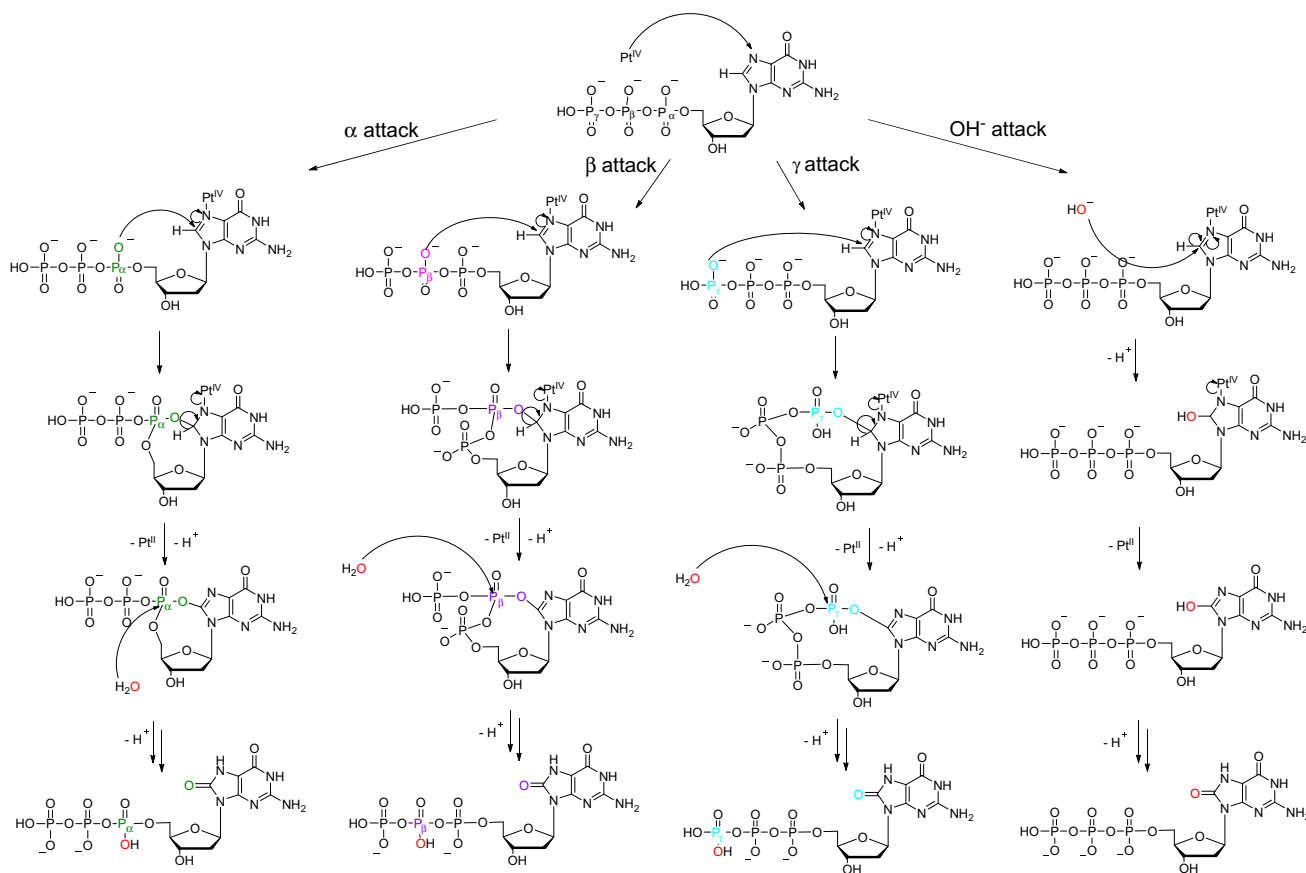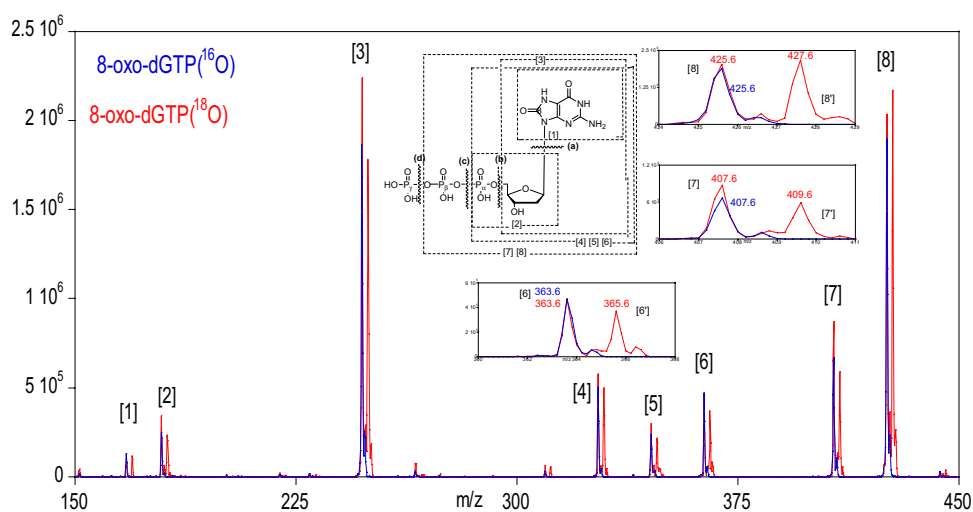
Scheme 4 Proposed mechanism for the oxidation of 5′-dGTP by [Pt^{IV}(dach)Cl$_4$] (represented as Pt^{IV}). [Pt^{II}(dach)Cl$_2$] is represented as Pt^{II}. The [Pt^{II}(dach)Cl$_2$] complex reacts further with excess 5′-dGTP and produces [Pt^{II}(dach)(5′-dGTP)$_2$]

followed by 5′-dGDP, and the slowest with 5′-dGTP. The change in A_{390} follows the exact same trend, with the maximum peak for 5′-dGMP (3.8 h) appearing earlier than that of 5′-dGDP (9.3 h), and of 5′-dGTP (14 h). This trend indicates

that the formation of an intermediate, Pt^{IV}–G, and its depletion by electron transfer initiated by intra- or intermolecular nucleophilic attack, occurs faster for 5′-dGMP, followed by 5′-dGDP, and last by 5′-dGTP. In our previous kinetic

Fig. 12 Changes in the electronic absorption at **a** 360 nm and **b** 390 nm over time, for the reaction of [Pt^{IV}(dach)Cl$_4$] (5 mM) with 5′-dGMP (50 mM), 5′-dGDP (50 mM) and 5′-dGTP (50 mM) in 100 mM NaCl at 35 °C with [Pt^{II}(dach)Cl$_2$] (0.02 mM) at a starting pH of 8.6 ($t = 0$)

Fig. 13 Change in the electronic absorption at **a** 360 nm and **b** 390 nm over time, for the reaction of [Pt^{IV}(dach)Cl$_4$] (5 mM) with 5′-dGTP (50 mM) with and without [Pt^{II}(dach)Cl$_2$] (0.02 mM) in NaCl (100 mM) at 45 °C and a starting pH of 8.6 ($t = 0$)
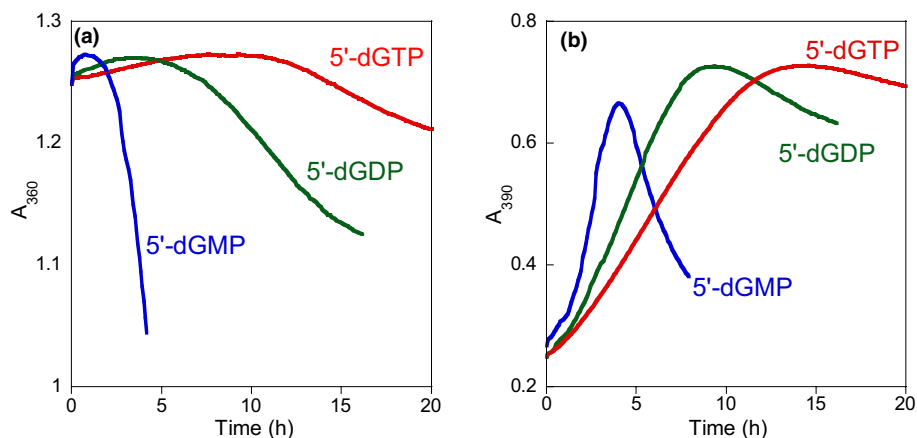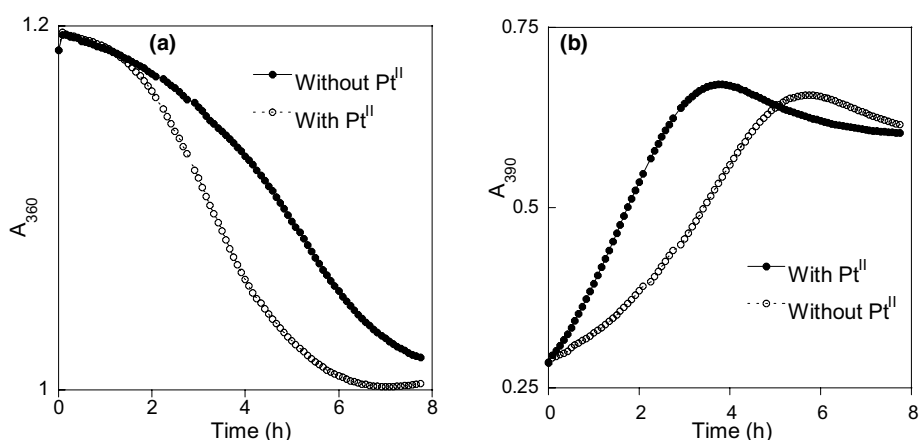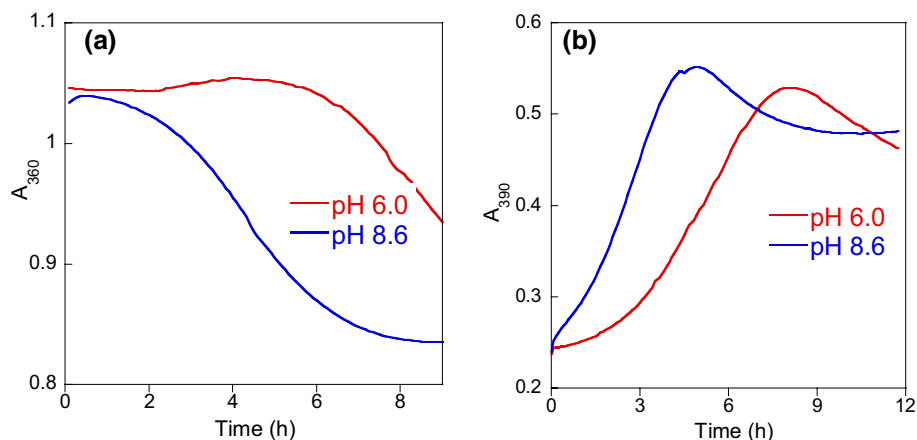
Fig. 14 Change in the electronic absorption at **a** 360 nm and **b** 390 nm over time, for the reaction of [Pt^{IV}(dach)Cl$_4$] (5 mM) with 5′-dGTP (50 mM) with and without [Pt^{II}(dach)Cl$_2$] (0.02 mM) in NaCl (100 mM) at 45 °C and a starting pH of 8.6 ($t = 0$) and 6.0 ($t = 0$

study on the Pt^{IV} reaction with 3′-dGMP and 5′-dGMP, we found that 3′-dGMP reacts faster than 5′-dGMP due to its low steric hindrance and low rotational barrier of 5′-group [21]. The activation parameters for the substitution and

electron transfer reactions of 5′- and 3′-dGMP indicated that the steric hindrance and the ability of the 5′-group to form H-bonds are the main factors influencing substitution, while the rotational barrier determines the electron transfer

step. Increasing the length of the phosphate chains should increase steric hindrance and rotational barrier, and decrease the overall reaction rate.

In previous studies, we also showed that the presence [$Pt^{II}(dach)Cl_2$] can catalyze the substitution reaction of [$Pt^{IV}(dach)Cl_4$] to 5′-dGMP, as shown in Scheme 2 [21]. Figure 13 shows the effect of the [$Pt^{II}Cl_2(dach)$] on the changes in A_{360} and A_{390} for the reaction of 5′-dGTP with [$Pt^{IV}(dach)Cl_4$] at 45 °C and at a starting pH of 8.6. The presence of [$Pt^{II}(dach)Cl_2$] shortened the induction time (Fig. 13a) and produced the [Pt^{IV}–G] intermediate at an earlier time than when the reaction was run without the catalyst (Fig. 13b). Similar results were obtained for 5′-dGDP (not shown). Therefore, we concluded that [$Pt^{II}(dach)Cl_2$] acts as a catalyst for the substitution reaction for both 5′-dGDP and 5′-dGTP.

Figure 14 shows the change of A_{360} and A_{390} for the reaction of 5′-dGDP with [$Pt^{IV}(dach)Cl_4$] at 45 °C and at two different starting pH values of 6.0 and 8.6. The changes of both wavelengths over time show that a decrease in pH from 8.6 to 6.0 significantly slows down the reaction. A decrease in pH leads to the protonation of the β-phosphate of 5′-dGDP, decreasing its ability to form H-bonds with the amine groups of [$Pt^{IV}(dach)Cl_4$] and thus decreasing the rate of substitution reaction, as well as decreasing the nucleophilicity of the β-phosphate group and thus slowing the electron transfer step. Therefore, lowering the pH decreases the overall reaction rate. However, another important aspect is the role of the intermolecular attack by free OH^- groups. A decrease of the pH from 8.6 to 6.0 lowers the concentration of free OH^- in the solution, decreasing the rate of intermolecular nucleophilic attack to $C_8[G–Pt^{IV}]$. Overall, the results from our kinetic study provide a qualitative framework to investigate in detail the factors that influence the reaction of [$Pt^{IV}(dach)Cl_4$] with 5′-dGDP and 5′-dGTP. The fact that the mechanisms for the reactions of 5′-dGDP and 5′-dGTP with [$Pt^{IV}(dach)Cl_4$] contain a greater number of intramolecular nucleophiles and cyclic phosphodiester intermediates, as well as a more significant role for the intermolecular nucleophiles than that of 5′-dGMP, will greatly increase the complexity of the quantitative kinetic studies.

Conclusion

The deprotonation of H_8-5′-dGMP bound to Pt^{IV} (H_8-G–Pt^{IV}) is not involved in the rate-determining step in the electron transfer between G and Pt^{IV}. The [$Pt^{IV}(dach)Cl_4$] complex oxidized 5′-dGDP and 5′-dGTP to 8-oxo-5′-dGDP and 8-oxo-5′-dGTP, respectively, by the same mechanism and kinetics as in the case of 5′-dGMP. The Pt^{IV} complex binds to N_7 followed by a two-electron inner sphere electron transfer from G to Pt^{IV}. The redox reaction was catalyzed by Pt^{II} and occurred faster at higher pH. The electron transfer was initiated by either an intramolecular nucleophilic attack by any of the phosphate groups or an intermolecular nucleophilic attack by free OH^- in the solution. The rates of reactions for the three nucleotides follow the order: 5′-dGMP > 5′-dGDP > 5′-dGTP, indicating that the bulkier the phosphate group, the slower the reactions, due to the larger steric hindrance and rotational barrier of the phosphate groups.

References

1. Schumacker PT (2015) Cancer Cell 27:156–157
2. Klaunig JE, Kamendulis LM, Hocevar BA (2009) Toxicol Pathol 38:96–109
3. Balaban RS, Nemoto S, Finkel T (2005) Cell 120:483–495
4. Mangialasche F, Polidori MC, Monastero R, Ercolani S, Camarda C, Cecchetti R, Mecocci P (2009) Ageing Res Rev 8:285–305
5. Abdel Moneim AE (2015) Curr Alzheimer Res 12: 335-349
6. Aslan M, Ozben T (2004) Curr Alzheimer Res 1:111–119
7. Steenken S, Jovanovic SV (1997) J Am Chem Soc 119:617–618
8. Muller JG, Kayser LA, Paikoff SJ, Duarte V, Tang N, Perez RJ, Rotica SE, Burrows CJ (1999) Coord Chem Rev 185–186:761–774
9. Burrows CJ, Muller JG (1998) Chem Rev 98:1109–1151
10. Clarke MJ, Morrissey PE (1984) Inorg Chim Acta 80:L69–70
11. Gariepy KC, Curtin MA, Clarke MJ (1989) J Am Chem Soc 111:4947–4952
12. Rodriguez-Bailey VM, LaChance-Galang KJ, Doan PE, Clarke MJ (1997) Inorg Chem 36:1873–1883
13. Choi S, Cooley RB, Voutchkova A, Leung CH, Vastag L, Knowles DE (2005) J Am Chem Soc 127:1773–1781
14. Choi S, Cooley RB, Hakemian AS, Larrabee YC, Bunt RC, Maupaus SD, Muller JG, Burrows CJ (2004) J Am Chem Soc 126:591–598
15. Choi S, Personick ML, Bogart JA, Ryu DW, Redman RM, Laryea-Walker E (2011) Dalton Trans 40:2888–2897. doi:10.1039/c0dt00822b
16. Choi S, Ryu DW, DellaRocca JG, Wolf MW, Bogart JA (2011) Inorg Chem 50:6567–6574. doi:10.1021/ic2003518
17. Wolf MW, Choi S (2012) J Biol Inorg Chem 17:1283–1291. doi:10.1007/s00775-012-0942-8
18. Noszal B, Scheller-Krattiger V, Martin RB (1982) J Am Chem Soc 104:1078–1081
19. Ariafard A, Tabatabaie ES, Aghmasheh S, Najaflo S, Yates B (2012) Inorg Chem 51:8002–8013. doi:10.1021/ic300038m
20. Chang R The chemical educator, vol. 2, No. 3: Springer: New York, 1997; pp 1–3
21. Choi S, Vastag L, Leung CH, Beard AM, Knowles DE, Larrabee JA (2006) Inorg Chem 45:10108–10114

22. Nakabeppu Y, Tsuchimoto D, Furuichi M, Sakumi K (2004) Free Radic Res 38:423–428
23. Schweizer MP, Chan SI, Helmkamp GK, Ts'O POP (1964) J Am Chem Soc 86:696–700
24. Kuzmic P (1996) Anal Biochem 237:260–273
25. Reily MD, Hambley TW, Marzilli LG (1988) J Am Chem Soc 110:2999–3006
26. Bose RN, Fonkeng BS, Moghaddas S, Stroup D (1998) Nucleic Acids Res 26:1588–1596
27. Robitaille PML, Robitaille PA, Brown GG, Brown GG Jr (1991) J Magn Reson 92:73–84